J. Fluid Mech. (1990), *vol.* 215, *pp.* 1–22
Printed in Great Britain

The interaction between a solitary wave and a submerged semicircular cylinder

By M. J. COOKER[1], D. H. PEREGRINE[1], C. VIDAL[2] AND J. W. DOLD[1]

[1]School of Mathematics, University of Bristol, Bristol BS8 1TW, UK

[2]Departomento di Ciencias y Tecnicas del Agua y del Medio Ambiente, Universidad de Cantabria, 39005 Santader, Spain

(Received 19 June 1989)

Numerical solutions for fully nonlinear two-dimensional irrotational free-surface flows form the basis of this study. They are complemented and supported by a limited number of experimental measurements. A solitary wave propagates along a channel which has a bed containing a cylindrical bump of semicircular cross-section, placed parallel to the incident wave crest. The interaction between wave and cylinder takes a variety of forms, depending on the wave height and cylinder radius, measured relative to the depth. Almost all the resulting wave motions differ from the behaviour which was anticipated when the study began. In particular, in those cases where the wave breaks, the breaking occurs beyond the top of the cylinder. The same wave may break in two different directions: forwards as usual, and backwards towards the back of the cylinder. In addition small reflected waves come from the region of uniform depth beyond the cylinder. Experimental results are reported which confirm some of the predictions made. The results found for solitary waves are contrasted with the behaviour of a group of periodic waves.

1. Introduction

The interaction of freely propagating water waves with obstacles is relevant to the design and operation of offshore and coastal structures. The study reported here arose from the continuing development of numerical methods and computer programs to model steep unsteady waves, including the initial stages of wave breaking. Our first computations of a solitary wave meeting an obstacle on the bed revealed unexpected behaviour and prompted this work.

Previous work on solitary waves meeting submerged obstacles discusses weak interaction in the context of shallow-water approximations such as the Korteweg–de Vries equation. Seabra-Santos, Renouard & Tempeville (1987) have examined the motion of solitary waves over triangular shapes. These theories predict some reflection, and a disturbed transmitted wave which leaves a small-amplitude dispersive wave train in its wake. Small, deeply submerged obstacles which are much shorter than the wavelength, are certainly inefficient at scattering long waves, and so long as one stays within the range of validity of the shallow-water equations such theories can only predict weak interactions. Our computations have allowed us to go further and investigate *strong* interactions between an object on the bed and a solitary wave.

The class of solitary waves was chosen for study because it includes the largest

steadily propagating wave in water of constant depth. Consequently it was thought that these might model the ocean waves most damaging to coastal structures.

A solitary wave propagating in water of constant depth h has properties that only depend on its height, a. A semicircular bump on the flat bed is described by its radius, R. This shape is chosen as a simple example of an obstacle that has dimensions which are of the same order of magnitude as the depth. We choose dimensionless units such that the depth of fluid h, gravity g, and the fluid density ρ are all unity. This leaves us with only two parameters in our problem: the wave amplitude a and the cylinder radius R. The (a, R) parameter space is limited by the maximum solitary wave height $a = 0.83$ and by our selection of *submerged* cylinders, hence R is less than one.

The primary method of investigation is computation of the water motion. The flow is approximated by two-dimensional irrotational incompressible inviscid flow, with no influence from the air movement above the free surface. We also neglect surface tension. The exact inviscid free-surface boundary conditions are used.

The numerical method is an extension of the boundary-integral program used by Tanaka *et al.* (1987) to study the stability of steep solitary waves. The program incorporates the high-order discretizations introduced by Dold & Peregrine (1986), and see also Dold (1990). The earlier program models waves propagating in fluid of fixed depth, and has been extended to describe wave motion over irregular beds. Some details of the method are given in §2. Suitable boundary-integral methods have been developed by Vinje & Brevig (1981), Teles da Silva (1989), and Yasuda, Hara & Tanaka (1990). They have also investigated solitary wave interaction with some submerged obstacles, but until now there has been no comprehensive discussion of the results such as that presented in this paper.

In §3 we summarize the computations which explore the (a, R) parameter space. A number of phenomena are found. Some are as expected: small obstacles cause small perturbations to the wave and bring about weak reflection, and waves that are so large initially that they are unstable are caused to break by small obstacles. Other behaviour is unexpected. Moderate size cylinders interact strongly with the wave. Over a wide range of parameters a second crest forms and quickly takes over from the incident crest. For large enough waves and cylinders, the waves break, but never while the crest is approaching the cylinder. The breaking always occurs beyond the top of the obstacle and often well past the whole obstacle. In addition some waves break backwards after passing the cylinder. Small reflected waves come from the uniform depth region *beyond* the cylinder. These unexpected results are described and discussed. Some are easier to interpret than others.

Experiments have been carried out for a limited number of examples of solitary waves propagating over semicircular bumps. These examples include breaking waves. Comparisons with computation proved satisfactory. The experiments are described in §4, and the experimental results are given in §5. Section 6 is a discussion of the computational and experimental results. Some conclusions are drawn in §7.

From a practical point of view, since none of our computations show any significant reflection of wave energy, the only way a submerged fixed† obstacle of this type can be an effective breakwater is when it induces wave breaking. Even then the breaking frequently occurs well beyond the cylinder and is restricted to a small region near the wave crest. Therefore, although our computations stop at the time of breaking it is likely that the transmitted wave continues its motion as a spilling breaker.

† Moving submerged obstacles can be very efficient wave energy reflectors, see Evans & Linton (1989).

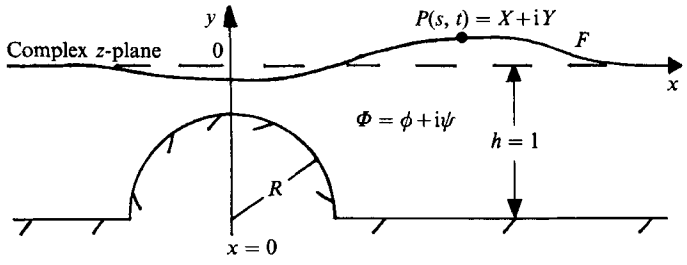

FIGURE 1. Definition sketch of physical plane. Lengths are scaled by the depth.

2. Mathematical Formulation

2.1. *The boundary-integral equation*

We assume that the fluid motion is two-dimensional, irrotational, inviscid and incompressible. The irrotational velocity field $\boldsymbol{u}(x, y, t)$ is the gradient of a velocity potential $\phi(x, y, t)$ which satisfies Laplace's equation in the fluid domain $\mathscr{D}$.

At the free surface, F, we impose the boundary condition that the fluid pressure is the same as the atmospheric pressure, p_0, above the fluid. We assume that p_0 is constant in time, and takes the same value along the entire length of F. For convenience we make $p_0 = 0$. We neglect surface tension. At infinity we suppose that the fluid surface is at rest at $y = 0$. Using Bernoulli's equation, with units chosen so that depth and the acceleration due to gravity are equal to unity, we have

$$\frac{\mathrm{D}\phi}{\mathrm{D}t} = \tfrac{1}{2}(u^2+v^2) - y \quad \text{on} \quad F, \tag{2.1}$$

where u, v are the components of the velocity $\boldsymbol{u}$, and y (measured vertically upwards) is the elevation of the free surface above the undisturbed water level.

$$\mathrm{D}/\mathrm{D}t = \partial/\partial t + \boldsymbol{u} \cdot \boldsymbol{\nabla}$$

denotes the time-derivative following the fluid motion.

We also impose the boundary condition that a fluid particle described by position vector $\boldsymbol{P}$ on the moving free surface F, remains on F. This kinematic boundary condition is

$$\mathrm{D}\boldsymbol{P}/\mathrm{D}t = \boldsymbol{\nabla}\phi \quad \text{on} \quad F. \tag{2.2}$$

On the fixed, impermeable bed we impose the condition

$$\partial\phi/\partial n = 0. \tag{2.3}$$

Lastly we have the far-field condition:

$$\boldsymbol{\nabla}\phi \to \boldsymbol{0} \quad \text{as} \quad x \to \pm\infty. \tag{2.4}$$

See figure 1. We solve Laplace's equation using a boundary-integral method, developed from that used by Tanaka *et al.* (1987) for solitary wave evolution over a flat bed at $y = -1$. That method is an extension of a version which is periodic in space, developed by Dold & Peregrine (1986). These programs achieve high computational efficiency owing to a number of factors, including high-order numerical approximations. A fully detailed account is in preparation, Dold (1990).

In the Tanaka *et al.* (1987) method the bed is a flat horizontal line. The image of the free surface in the flat bed at $y = -1$ is used, and Cauchy's integral theorem, in

principle value form, is applied to the complex velocity Φ_z on F: $\Phi_z = \phi_x - \mathrm{i}\phi_y = (\phi_s - \mathrm{i}\phi_n) P_s^*/|P_s|^2$,

$$\pi\phi_n(s) = \int_F \phi_s' \,\mathrm{Re}\left\{\frac{P_s}{P'^* - 2\mathrm{i} - P} - \frac{P_s}{P' - P}\right\} \mathrm{d}s' - \int_F \phi_n' \,\mathrm{Im}\left\{\frac{P_s}{P' - P} + \frac{P_s}{P'^* - 2\mathrm{i} - P}\right\} \mathrm{d}s'. \quad (2.5)$$

In (2.5) $P = X + \mathrm{i}Y = P(s,t)$ is a complex number describing the position of a fluid particle on F, and s is a real variable which parametrizes the free surface: F is described by s in a clockwise sense, i.e. from $x = -\infty$ to $x = \infty$. A prime indicates evaluation at s', and the absence of a prime indicates evaluation at s. $P_s = \partial P/\partial s$ at s, and * signifies complex conjugate. ϕ_n is a scaled derivative along the outward-drawn normal to the free surface, and ϕ_s is a scaled tangential derivative. The integrals are principal value.

Note that s is not necessarily arclength, and here we choose s to vary along F so that it has integer values at discretization points.

We can summarize the basic, obstacle-free method in two steps: initial position (X, Y) and potential $\phi(P)$ known at the surface, at time t.

(1) Solve (2.5) for ϕ_n the derivative normal to the free surface.

(2) Time-step X, Y, ϕ from time t to $t + \Delta t$ using (2.1) and (2.2).

In step 2 the computation points P follow the fluid motion, and coincide with fluid particles on F. The concise way in which we are able to present the integral equation is due to the reflection of the free surface in the *flat* bottom. For an irregular bed we cannot do this immediately. So first we conformally map the physical plane of figure 1 into a domain containing a flat bed. The mapping preserves Laplace's equation in the transformed variables. The image of the free surface, under the conformal mapping, can then be reflected in the flat bed, and the integral equation solved. The solution is conformally mapped back into the physical plane for the time-stepping process. The benefits of solving Laplace's equation in a flat-bedded plane are important: the use of images avoids integration along the bed.

To summarize, we have a four-stage method for irregular beds to replace the above two-stage scheme for flat beds: the two additional steps consist of the conformal mapping (step 1) and its inverse (step 3): Initial position of surface (X, Y) and potential $\phi(P)$ known at time t.

(1) Conformally map X, Y, ϕ to $\bar{X}, \bar{Y}, \bar{\phi}$ in flat-bedded plane.

(2) Solve for $\bar{\phi}_n$ using (2.5) (expressed in overbarred variables).

(3) Conformally map $\bar{X}, \bar{Y}, (\bar{\phi}_s, \bar{\phi}_n)$ back to physical plane: $X, Y, (\phi_s, \phi_n)$.

(4) Time-step X, Y, ϕ from time t to $t + \Delta t$ using (2.1) and (2.2).

If N is the number of surface computation points then $O(N^2)$ operations are needed to set up and solve the integral equation (2.5), for each time-step. This is because we use an iterative scheme to solve the linear system. A direct method of solution would have involved $O(N^3)$ operations. The conformal transformations at steps 2 and 4, in the program involve $O(N)$ operations and so they represent a small overhead in the cost of computation, even if a complicated mapping is required.

2.2. *Numerical method*

The fluid domain $\mathscr{D}$ is truncated at the left- and right-hand ends of the flow, the 'end' being defined where the surface elevation is found to be less than 10^{-5}. The truncated

free surface F is discretized using N points. The parameter s at time t describes F, i.e. $P = P(s,t) = X(s,t) + \mathrm{i}Y(s,t)$. We choose the parametrization such that s takes on integer values at the N computation points, and so s is a point label parameter.

With this choice of s we can turn (2.5) into a system of linear equations for the set of unknowns $\{\partial\phi/\partial n\}_{s=1,N}$, provided we pay due care to the evaluation of the integrals near $s' = s$ (i.e. near $P' = P$):

$$\phi_n(s) = -\frac{1}{\pi}\phi_{ss}(s) + \frac{1}{\pi}\sum_{s'=1}^{N} A(s,s')\,\phi_s(s') + \frac{1}{\pi}\sum_{s'=1}^{N} B(s,s')\,\phi_n(s'), \tag{2.6}$$

where

$$A(s,s') + \mathrm{i}B(s,s') := \left\{\frac{P_s}{P'^* - 2\mathrm{i} - P}\right\}^* + \begin{cases} \dfrac{P_s}{P-P'} & :s' \neq s \\ \dfrac{P_{ss}}{2P_s} & :s' = s. \end{cases} \tag{2.7}$$

A prime denotes evaluation at s', and the absence of a prime denotes evaluation at s. The real matrices A and B are $(N \times N)$. The singular parts of the integrand of (2.5) manifest themselves in the components $P_{ss}/2P_s$ of $A + \mathrm{i}B$, in (2.7). The remaining parts of the integration are estimated by the trapezoidal rule and appear in the summations. Note that the free surface is almost flat for a significant region at each end of the domain and so both ϕ_s and ϕ_n are very small at the limits of integration. Further, it is a convenient fact that neighbouring points have unit separation when described in s-space. The trapezoidal rule is then accurate to a high order when used to integrate functions, such as those in (2.5), which are tending to zero at each end of the domain.

Equation (2.6) can be solved iteratively for $\{\phi_n(s)\}_{s=1,N}$ (see Dold & Peregrine 1986). The first estimate for $\{\phi_n\}$ is found by calculating the right-hand side of (2.6). In the first summation of (2.6) we use $\{\phi_s(s')\}_{s'=1,N}$ calculated at the current time. A good first iterate, in the interation process to find $\{\phi_n(s')\}_{s'=1,N}$, is to use the solution found at the previous time-step. This old solution is used in the second summation of (2.6).

The tangential derivatives are estimated by eleven-point central difference formulas, based on the values $\phi(s), \phi(s\pm1), \ldots, \phi(s\pm5)$. These very accurate estimates ensure that the overall method is precise and robust. The first estimate for $\{\phi_n\}$ is substituted into the right-hand side of (2.6) to find the second iterate, and so on, until successive iterates differ by less than a fixed parameter. Convergence is normally achieved within less than 16 iterations. We now know (ϕ_s, ϕ_n) at time t, at each computation point, so we can use (2.1) to find $\mathrm{D}\phi/\mathrm{D}t$.

Equation (2.2) is an ordinary differential equation in time for the surface position. A Taylor series expansion about time t enables us to integrate this ODE over the time-step t to $t+\Delta t$, and the higher time-derivatives of ϕ are found as follows. The first and second time-derivatives, $\phi_t(t)$ and $\phi_{tt}(t)$, also satisfy Laplace's equation. Once ϕ_t has been calculated from Bernoulli's equation, we can repeat the above method to find (ϕ_{tn}, ϕ_{ts}), (ϕ_{ttn}, ϕ_{tts}) and hence $\mathrm{D}^2\phi/\mathrm{D}t^2$, $\mathrm{D}^3\phi/\mathrm{D}t^3$ at time t. $\mathrm{D}^4\phi/\mathrm{D}t^4$ and $\mathrm{D}^5\phi/\mathrm{D}t^5$ are also estimated, from backward difference formulas involving the values of $\mathrm{D}^3\phi/\mathrm{D}t^3$ at the two previous time-steps. Using (2.2) we can time-step the fluid surface from its position at time t, to its position at time $t+\Delta t$, and use (2.1) to find the new values of ϕ at the new surface position. So in effect we use a fifth-order Taylor series in time to perform the time-stepping.

2.3. *Application of the method: the semicircular breakwater*

An example of the application of the above method is a bottom which consists of a semicircle placed on an otherwise flat horizontal bed. See figure 1. The bump has centre $z = -\mathrm{i}$ and radius R, in a depth of fluid $h = 1$. A conformal transformation which maps this profile into a flat-bedded plane is

$$w = z + \frac{R^2}{z+\mathrm{i}}, \tag{2.8}$$

where w is a complex variable describing a flat-bedded plane such that $\mathrm{Im}\,(w) = -1$ on the bed.

The initial conditions are a solitary wave of height a on unit depth of fluid propagating in the $-x$ direction towards the cylinder. The initial wave is calculated using the method of Tanaka (1986) and is placed so that the surface elevation at the cylinder is less than 0.001 of the depth.

We make distances and times dimensionless by scaling with respect to the depth h and $(h/g)^{\frac{1}{2}}$, respectively. With reference to these scales the incident solitary wave has an amplitude $a < 0.83$, and the radius of the semicircle $R < 1$.

As few as 35 computation points placed along the free surface can describe the steady propagation of a solitary wave of amplitude 0.2. For larger solitary waves up to amplitude 0.8 more points are needed, rising to around 85 for the highest. Solitary waves with height less than 0.1 are also very long so more points are needed to describe the tail of the wave. In the initial data for the wave, the density of points is greater near the crest than in the tail. In a frame of reference moving with the wave, fluid particles move more slowly at the crest than in the tail. The initial point separation is made directly proportional to this local fluid speed along the free surface, and so the point density is maintained naturally by the fluid motion when the wave is propagating steadily (New 1983 and Peregrine 1990).

As the wave travels forward, extra points are added onto the front of the domain. A new point is added if the end point has moved vertically further than 10^{-5} from $y = 0$. The new point is placed at $y = 0$ and at a distance equal to the separation of the last two points. A similar process removes computation points from the tail end of the domain.

The length of each time-step is controlled during calculation by the algorithm so it is not easy to compare with other methods which have fixed time-steps. The time-step is chosen as follows. Consider the term $(\Delta t_3)^3\,(\mathrm{D}^3\phi/\mathrm{D}t^3)/3!$ in the Taylor series expansion for $\phi(t+\Delta t)$. We require that Δt_3 be chosen such that the largest value of this term, over the set of points in F, must be ϵ, a precision parameter. Similarly Δt_4 is the time-step which limits the largest fourth-order term over F to ϵ. The time-step is then chosen to be $\Delta t = (\Delta t_3 \Delta t_4)^{\frac{1}{2}}$.

For a steadily propagating solitary wave of height 0.5, 10 time-steps are needed for each unit of time when $\epsilon = 10^{-5}$. When there are 85 points, in the absence of any obstacle, 10 time-steps require the following.

Machine	CPU Time (s)
IBM 3090-150S (with vector processing)	0.5
Gould NP1	5
VAX 750	30
IBM-Compatible Tandon AT PC (with 80287 coprocessor)	100

The time-step shortens by approximately 40 % when the crest is near the obstacle because of the more irregular surface motion. The method is stable. It does not suffer from saw-tooth instabilities.

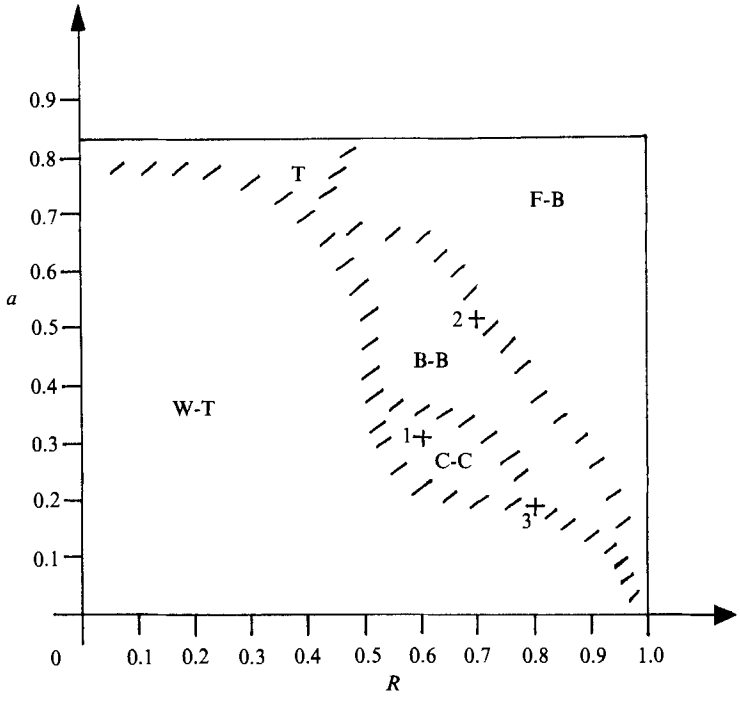

FIGURE 2. The (a, R) parameter space. a and R are the dimensionless incident wave amplitude, and semicircle radius, respectively. The symbols (+) indicate experiments.

Throughout the calculations for this paper the mass changed by less than 10^{-4} of the initial mass of fluid above $y = 0$. Changes in the total energy amounted to less than 10^{-5}. As a check on the computations, the same semicircular bed shape was used in another program which places discretization points on that part of the bed which is not horizontal, instead of using a conformal map. The comparison involved a solitary wave of height 0.5 running over a semicircle of radius 0.5, and was carried out courtesy of F. Teles da Silva. The programs computed ten time units and after this time the (x, y)-components of surface position were found to differ only in the fifth significant figure.

Inspection of local accelerations and pressure gradients shows that accuracy becomes poor once surface features have lengthscales as short as the point separation. For example consider a steady flow over a submerged obstacle which produces downstream very short, stationary waves. Deep-water waves of length 0.063 are stationary on a stream of speed 0.1, in unit depth. Any waves of this length are too small to be resolved except by an unreasonably large number of computation points, yet the unsteady flows described here can be expected to generate such waves. We have not considered it worthwhile to pursue such minor features of the flow.

3. Computational results

In this section we discuss the results of computations which cover the complete range of wave heights and cylinder radii. The (a, R) parameter space contains regions of different wave response. See figure 2, which summarizes the explorations involving about 130 separate computations. The regions have appreciable overlap, because

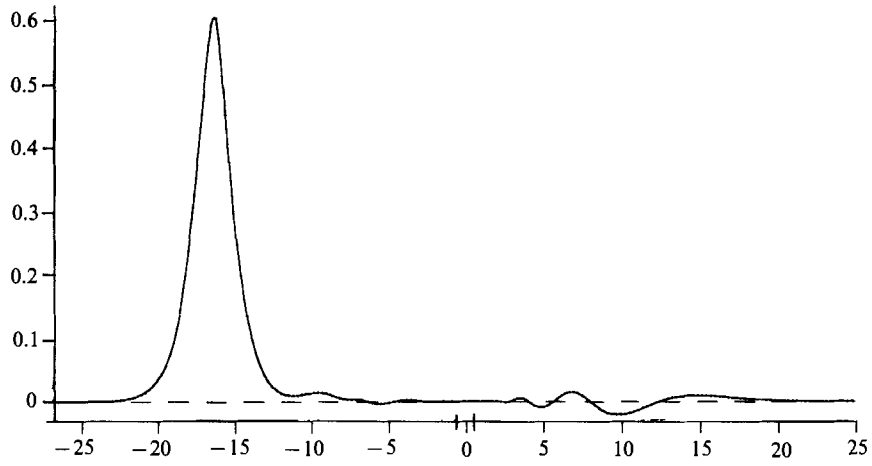

FIGURE 3. $a = 0.6, R = 0.5$. Wave train: W-T. Incident wave moves from right to left. Transmitted wave, with dispersive waves trailing behind, and right-travelling reflected waves. Vertical exaggeration = 40. Position of semicircle shown, with centre at $x = 0$.

more than one response may occur for a given combination of wave height and semicircle radius. Only the first significant response is plotted in the figure. The principal phenomena of interest within each region are described below.

3.1. *Wave train (W-T)*

The large region labelled W-T in the lower left part of figure 2 represents the interaction between solitary waves and small to medium size cylinders. The region is characterized by the solitary wave being only slightly perturbed by the obstacle. The transmitted wave carries behind it a small dispersive wave train. There is also a train of reflected waves.

Figure 3 illustrates this for a wave of height 0.6 which has passed over a cylinder of radius 0.5. The surface profile has been vertically exaggerated to show the smaller trailing and reflected waves. The reflected wave has a near-zero mean surface elevation, so it cannot evolve into a solitary wave of any significant height. Note the equally small wave at $x = -10$ in the tail of the solitary wave, which may evolve into a secondary wave, because it has a small, positive mean surface displacement.

Seabra-Santos *et al.* (1987) investigated experimentally the problem of solitary wave propagation over an isolated triangular obstacle. In one set of experiments the obstacle had height 0.4 and base width 0.564. The incident waves lay in the range $a = 0.2$ to $a = 0.6$, and each showed a small reflected solitary wave. From their figure 10 one can infer a reflection coefficient of approximately 0.05 for a wave of height 0.4. (Contrast this with the smaller reflection coefficient of 0.03 for the computation above in which $a = 0.6$ and the obstacle is larger: $R = 0.5$). There were no solitary waves in the wake of their transmitted wave. The triangular obstacle and our larger semicircle both produce a dispersive wave train and a reflected wave. Seabra-Santos *et al.* comment that for obstacles smaller than half the depth the reflected waves are negligible. The discrepancy in the size of these very small secondary waves may be accounted for by the difference in shape between the obstacles, and real fluid effects, such as flow separation, which might reduce reflection in experiments.

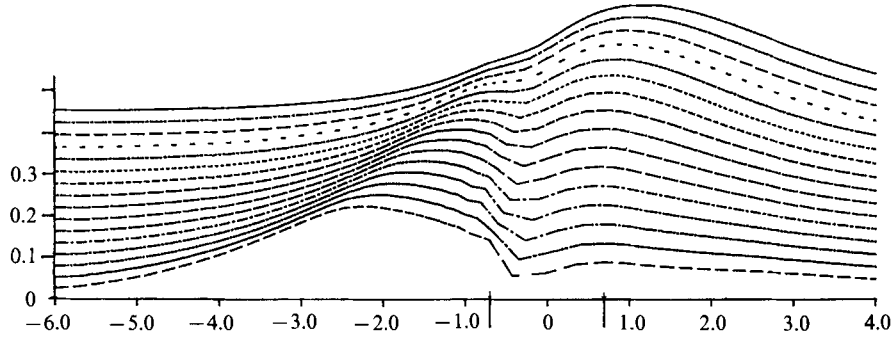

FIGURE 4. $a = 0.219$, $R = 0.7$. Crest exchange: C-C. The incident wave decreases in amplitude while, on the opposite side of the obstacle, the transmitted crest grows. Vertical exaggeration = 5. Obstacle position as shown. The last few profiles show that the discretization cannot resolve the very short waves generated by the flow. Times $t = 6.0, 6.2, \ldots, 9.0$. Time increases down the page.

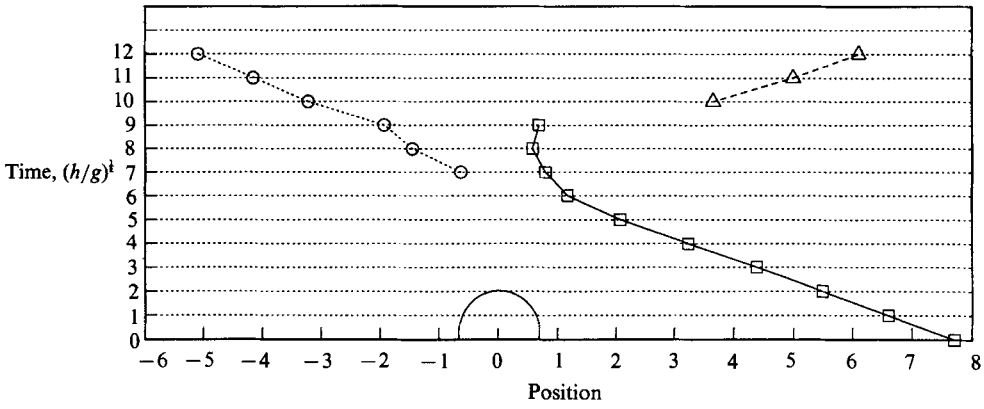

FIGURE 5. As figure 4. Position of crests in time. The incident crest (——) amplitude vanishes at $t = 9$. Transmitted wave (· · · · · ·) has amplitude 0.223 at $t = 12$; reflected wave (– – – – –) has amplitude 0.04 at $t = 12$.

3.2. *Crest–crest exchange (C-C)*

Almost all solitary waves of amplitude greater than about 0.2, riding over cylinders larger than about $R = 0.5$, exhibit a double crest as they cross the obstacle. The incident wave approaches the cylinder and a bulge grows in the surface, on the opposite side of the obstacle. The bulge grows into the crest of a new wave which propagates away from the obstacle. While the new crest grows, the incident crest decays to a fraction of its original height, and slows down. Then its direction reverses and it propagates away as a small reflected wave. This effect we call *crest–crest exchange*, and it dominates the interaction in the regime labelled C-C in figure 2. It also occurs in much of the regions marked F-B and B-B, where other types of interaction are more important. We have adopted the name 'crest-crest exchange' because the wave appears to exchange one crest for another in a short period of time.

Figure 4 illustrates this effect for an example where $a = 0.219$ and $R = 0.7$. The path of each crest is plotted in the space–time diagram of figure 5. The height of each crest is also indicated. Figure 5 is in part reminiscent of a space–time diagram for a solitary wave overtaking a smaller one where, unless there is a large disparity in size, the two crests remain distinct and exchange identities.

The long solitary wave passing over the short cylinder induces a flow over the semicircle which varies slowly in time. It is reasonable to ask if the disturbances in the free surface, induced by the wave, bear any resemblance to the disturbances induced by a steady flow passing over the semicircle.

Consider a flow such that at $t = 0$ the free surface is at $y = 0$, above the semicircle. At all times, at $x = \pm\infty$, the flow is from right to left with speed c. We have modified the numerical method to model the unsteady development of the free surface. For the small values of c that we consider here, stationary waves are found to develop downstream of the semicircle. As time goes on successive wave crests form ever-further from the obstacle. The situation that arises as $t \to \infty$ has been discussed within the context of a steady flow theory by Forbes & Schwartz (1984).

We choose a value of c appropriate for comparison with the flow induced by the passage of the solitary wave. For the solitary wave problem the maximum horizontal mass flux over the cylinder was 0.4. In the steady upstream flow problem the fluid flowing over the top of the $R = 0.7$ cylinder has depth 0.3. So to gain a mass flux of 0.4 we need $c = 0.3 \times 0.4 = 0.12$. Also the solitary wave sustains the near-maximum flow over the semicircle for about three time units, so it is reasonable to let the steady flow pass for a similar period of time. Over three time units we found that the steady upstream flow induces a depression of amplitude 0.04 and length 0.9 over the obstacle, and also part of the first wave in the wave train. The amplitude and wavelength (0.04 and 0.9) of the depression match the dimensions of the trough between the two crests in figure 4.

A full discussion of the problem of the steady and unsteady waves induced by a uniform upstream flow, is given by Teles da Silva (1989), using a method related to that used here.

3.3. *Backward breakers (B-B)*

In the region of figure 2 labelled B-B we have solitary waves of amplitude between 0.3 and 0.5 passing over cylinders of radii 0.5 to 0.7. After the main crest has passed over the obstacle, the surface in the tail of the wave, and near the obstacle, steepens and breaks *backwards* onto the cylinder. This breaking in the transmitted wave's tail also occurs for parameters in the region labelled F-B, discussed below. However, B-B is characterized by backwards breaking occurring before any other breaking event.

An example of a backward breaker is given in figure 6 which shows the sequence of profiles for a solitary wave of height 0.462 passing over an obstacle of radius 0.7. The forward face in the transmitted wave is steeper than that of the incident wave. The rear part of the wave steepens and forms a new crest that breaks backwards towards the cylinder, well after the main crest has cleared the obstacle. See figure 6(*b*).

The numerical method fails when there are insufficient computation points to resolve profiles containing points of high curvature, or when the distribution of values of ϕ becomes too irregular to form accurate tangential derivatives. This has occurred at the point of backward breaking.

The backward breaker is caused by the flow over the obstacle due to the transmitted wave. A steady flow over a semicircular obstacle induces a steady downstream disturbance as discussed above. For small cylinders and moderate flows this disturbance is a train of stationary waves propagating at speed c on a current of speed $-c$. Our backward breaker may be the first wave in such a wave train caused by the unsteady flow of the passing wave. As the transmitted wave recedes any such waves become free to propagate towards the cylinder. The first wave either steepens

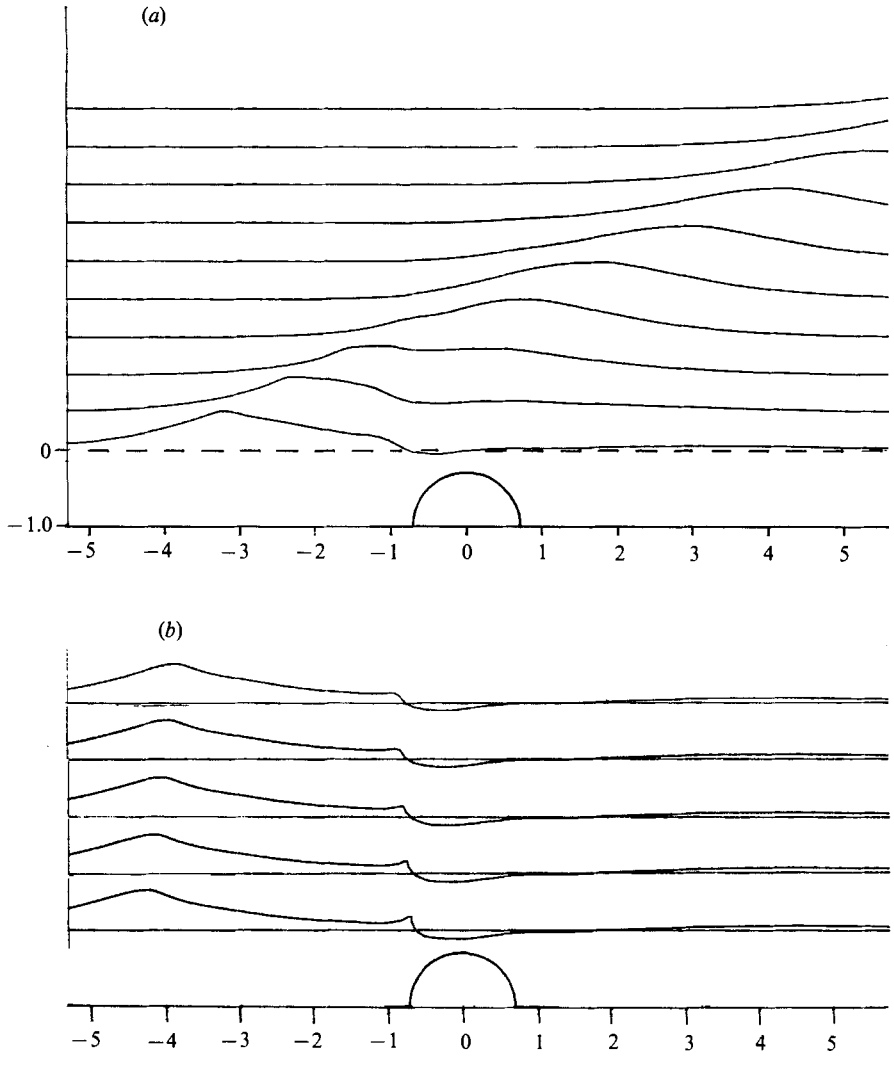

FIGURE 6. $a = 0.462$, $R = 0.7$. Backward breaking: B-B. Transmitted wave moves right to left. (*a*) $t = 0, 1, 2, \ldots, 9$. (*b*) Final stages of breaking: $t = 9.6, 9.7, 9.8, 9.9$.

sufficiently to break, or simply travels over the obstacle. Whether or not the wave breaks, the net effect is a wave reflection which appears to originate in the region of uniform topography beyond the cylinder. A more clear-cut example of the generation and reflection of waves by this type of mechanism is documented by New, Dyer & Lewis (1986, 1987), and see New & Dyer (1988). These papers report field measurements of internal waves on a pycnocline, in an estuary. The tidal flow generates a stationary wave train behind an irregularity of the bed and as the tide slackens the stationary waves become free to propagate.

Unlike the small wave in the discussion on C-C above, the solitary waves in B-B are larger. Consequently they may be able to induce more than one disturbance of wave-train type, and with greater amplitude. We investigated the type of disturbances induced by uniform streams at infinity passing over a semicircle of radius 0.7, similar to those calculations discussed for C-C. The maximum flow

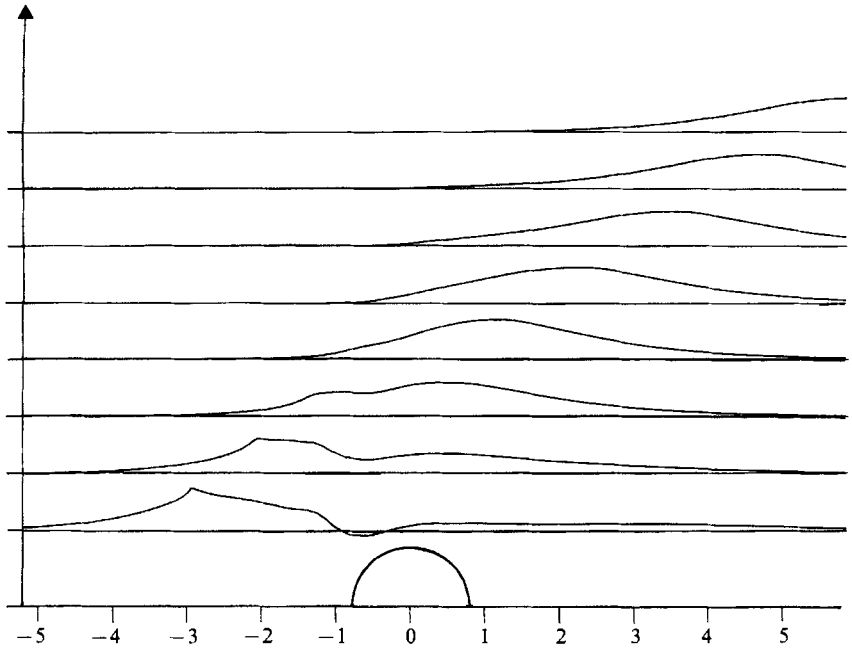

FIGURE 7. $a = 0.462$, $R = 0.8$. Forward breaking: F-B. The wave breaks well beyond the obstacle. $t = 0, 1.0, 2.0, \ldots, 7.0$.

velocity over the obstacle is 0.6 which corresponds to a uniform flow at infinity of 0.42. The free surface deforms in two time units into a steep downstream wave which breaks backwards onto the semicircle. This strongly suggests a connection between the flow over the semicircle and the unsteady backward breaker. However, it does suggest that our backward breaking may be best thought of as the natural, forward breaking of an incipient stationary wave. On the other hand, the greater heights of the incident solitary waves in B-B make the quantitative comparison with a steady upstream current over an obstacle, more difficult than the comparison made for C-C.

3.4. *Forward breakers (F-B)*

If we increase either the wave height or cylinder radius from the values for the region B-B the front of the transmitted wave breaks. This zone F-B in (a, R) space (figure 2) is characterized by the forward breaking of the transmitted wave. Note that surface steepening in the rear part of the wave, which may lead to the backward breakers of B-B, also occurs, but F-B is characterized by the forward breaking occurring before any backward breaking.

Figure 7 is a sequence of profiles for a wave of height 0.462, travelling over a cylinder of radius 0.8. At the last stage the wave is breaking, and the computations can no longer resolve the motion. In these circumstances the transmitted wave does not resemble a solitary wave. There is a close similarity to figure 6(*a*) where the same wave meets a slightly smaller cylinder. Note that the transmitted wave breaks far from the obstacle, and that it is only 0.55 in height; well below the theoretical height at which a solitary wave is unstable.

Forwards and backward breaking can occur simultaneously. For the wave of height 0.462 discussed here, the main crest breaks forward at the same time as the second crest breaks backward, if R is 0.77.

The largest waves ($a > 0.7$) and the biggest cylinders ($R > 0.9$) produce extreme examples of forward breaking which are close to the cylinder, and occur while the unbroken incident crest is over the obstacle. The breaking is a very localized phenomenon and hardly disturbs the incident crest or its tail. Intuitively one expects a wave to break where the depth is decreasing, in front of the obstacle. However, at all points in the parameter space where waves break they do so beyond the top of the cylinder. Even in extreme situations the breaker forms to the left of the cylinder's centreline.

3.5. *Tanaka instability* (T)

A rule of thumb learnt from the wave-train region W-T of figure 2 is that small semicircles up to a radius of around 0.5 have little effect on waves passing over them. However, this is only true of waves up to a height of about 0.78. At the top of figure 2 is a region marked T in which small obstacles induce wave breaking. Solitary waves bigger than 0.78 are disturbed by small cylinders. The disturbance grows as the wave propagates away from the obstacle until, five or six depths away, the wave breaks at its crest. In this part of (a,R)-space most waves are higher than the wave of maximum energy (height $a_e = 0.78066$). Tanaka (1986) shows that a_e marks the lower boundary of instability. The evolution of the disturbance is similar to that shown by Tanaka *et al.* (1987). It would be surprising if this instability were *not* triggered by the cylinder.

Two types of finite-amplitude evolution occur for Tanaka's instability. According to the sign of the coefficient of the unstable eigenfunction in the perturbation, a wave higher than a_e can either break or smoothly evolve into another solitary wave of the same energy and height less than a_e. It seems likely that a perturbation due to a dip in the bed may lead to the latter type of evolution. Further, in so far as Tanaka's instability may be related to wave breaking on a beach, this instigation of breaking by an elevation in the bed suggests that the non-breaking evolution is unlikely in shoaling water.

4. Experiments

Experiments were carried out in a wave tank to check the above numerical predictions. The tank was 70 m long and 2 m wide with a piston-type hydraulically operated wave maker at one end, and a beach at the other end which damped out extraneous wave disturbances. The wave maker was capable of forming solitary waves up to a height of approximately 0.52 at the obstacle, in the depths of water we used. The concrete bed of the tank deviated by less than 2 mm from a flat level plane. See figure 8.

Each wave was allowed to propagate a horizontal distance of about 40 m (approximately 150 depths), in a constant-depth region, before it reached the test section. This allowed the solitary wave to draw well ahead of any other waves generated by the wave maker. Since the wave had to propagate a long way, viscous dissipation caused the wave height to decay by 20% for the largest waves, and less for the smaller. The incident wave height was measured 2 m in front of the submerged obstacle. Further wave height loss due to viscous effects over the last 2 m was considered to be negligible, and that 2 m was far enough in front of the cylinder for the wave to have not yet been affected by it. Between each experiment the water surface was continuously monitored until there were no waves present larger than 0.2 mm. Very long standing waves were the slowest to decay and took up to 30 minutes to disappear.

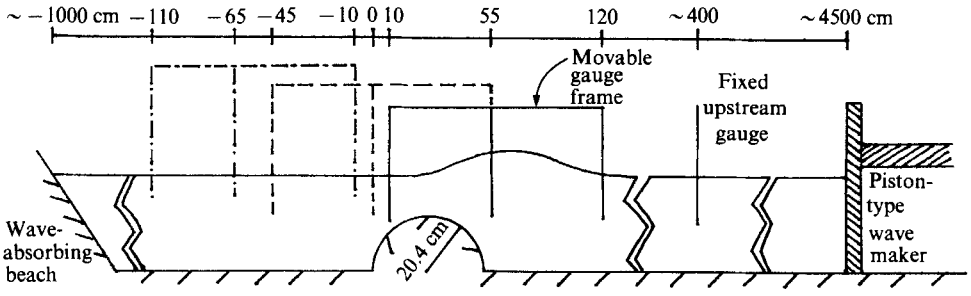

FIGURE 8. Schematic diagram of wave tank.

We used capacitance wave gauges, placed vertically through the water surface. The gauge registered the depth every 0.0351 s over a period of about 10 s. The upstream gauge measured the height of the incident wave, and this gauge remained fixed throughout the experiments. All the wave gauges were placed close to the centreline of the channel, which was a partitioned subsection of the tank about 60 cm wide. Limitations on the data capture equipment prevented use of more than three gauges, along with the fixed upstream gauge. This restriction on the number of gauges made it necessary to generate a wave, move the gauges, and then generate the same wave again. By making three runs of the same wave local surface elevations, as a function of time, were obtained at nine positions (two of which coincided just to the right of the obstacle), as shown in figure 8. The three gauges were fixed relative to each other, and placed on a movable carriage so as to make swift and accurate positioning easier.

Ideally the three incident wave heights (as measured at the upstream gauge) would have been the same. However, the heights were found to vary by up to 5% of the mean value. To allow for this, the corresponding computations were carried out using the three different incident wave heights, as measured at the upstream gauge. So our computations conform as closely as possible to the circumstances of the experiments. A video record was also made of the surface motion near the cylinder.

The cylinder was a concrete drain pipe (204 mm in radius), sawn down its length, and cemented to the concrete bed of the wave tank. The pipe was positioned so that the cross-flume variation in fluid depth over the pipe was nowhere more than ± 1 mm. The fluid motion was observed to be uniform across the tank width, and there were no spurious waves reflected between the partition walls.

We chose to examine the effects of three non-dimensional cylinder radii: $R = 0.6$, 0.7, and 0.8. The value of R was varied by altering the depth of water. The depths used for the 204 mm cylinder were 340, 291, and 255 mm with an error of ± 0.5 mm.

There are several sources of error. The gauges have an accuracy of ± 0.1 mm. The video record showed that the passage of the larger waves caused about ± 1 mm horizontal movement of the gauges at the level of the surface. The movement occurred because the lower end was left free, in order to minimize the disturbance to the flow. This horizontal motion is only significant when the free surface is steep. There may also have been hysteresis in the gauge responses due to wetting of the gauges as the water surface fell. This source of error can be quantified by examining the record made at the upstream gauge, where the gauge should have registered a symmetric response, if we assume that the experimental waves were spatially

symmetric. The experimental and computational initial data were found to disagree by much less than one symbol size in the figures showing results below.

5. Experimental results

The values of incident wave height and cylinder radii chosen for the experiments are shown in figure 2. Figures 9(*b*) to 11(*b*) show graphs of the local surface elevation at the wave gauges, as a function of time. Both axes are in non-dimensional variables. The experimental results are shown as discrete symbols and our numerical predictions as continuous lines. Error bars on the data would be about the same size as the symbols when the surface is nearly horizontal, and about five times the symbol size when the local surface slope is 45°.

In each example, only one representative set of measurements is shown. Each set of measurements corresponds to one of the three positions in which the gauge carriage was placed. The three gauges on the carriage measured the wave as it passed through the experiment. The sets of records of the other two gauge carriage positions, with their slightly different waves, are not shown, even though some show closer agreement with the computations than the results presented.

The positions of the wave gauges are given in figures 9(*a*) to 11(*a*). The symbol drawn over each gauge position corresponds to the symbol used to plot the experimental data in figures 9(*b*) to 11(*b*). Figures 9(*a*) to 11(*a*) also show the corresponding sequences of computed wave profiles (the waves move from right to left). All the graphs 9, 10 and 11 are vertically exaggerated by a factor of eight. The exaggeration distorts the semicircular obstacle into an ellipse.

5.1. *Example* 1

The first example (see figure 9*a*, *b*) illustrates a wave which did not break at any time and exhibited the phenomenon of crest–crest exchange across the obstacle (C-C). The cylinder radius R was 0.6 and the incident wave height a was 0.311.

There is good agreement between theory and experiment throughout the simulation time for those gauges away from the semicircle. For gauges near the obstacle, the agreement is good up to time 8, by which time the crest has passed the gauge. Afterwards our computations predict small-scale disturbances close to the obstacle, not recorded in the wave tank. It is likely that the flow over the semicircle separates, leading to these differences in small-scale behaviour. In addition the numerical scheme may be less reliable since the computation points in this region become widely separated (up to a distance of 0.3) by the flow.

The peak response and its timing for all three gauges are in close agreement with our theory. Also the main phenomenon of crest exchange across the obstacle has been accurately predicted, and can be seen in figure 9(*b*) from the lower peak response at gauge position $+$, relative to the peaks at gauges ∇ and $\triangle$.

5.2. *Example* 2

Figure 10(*a*, *b*) shows an example of the phenomenon of forward breaking (F-B in figure 2). In figure 2 the example (which is a cross labelled 2) is seen to lie on the border of the regions F-B and B-B. The initial stages of backward breaking occurred in the experiment. The cylinder radius R was 0.7 and a was 0.514. The waves used in this experiment were nearly the largest which could be made in the tank at the water depth of 291 mm.

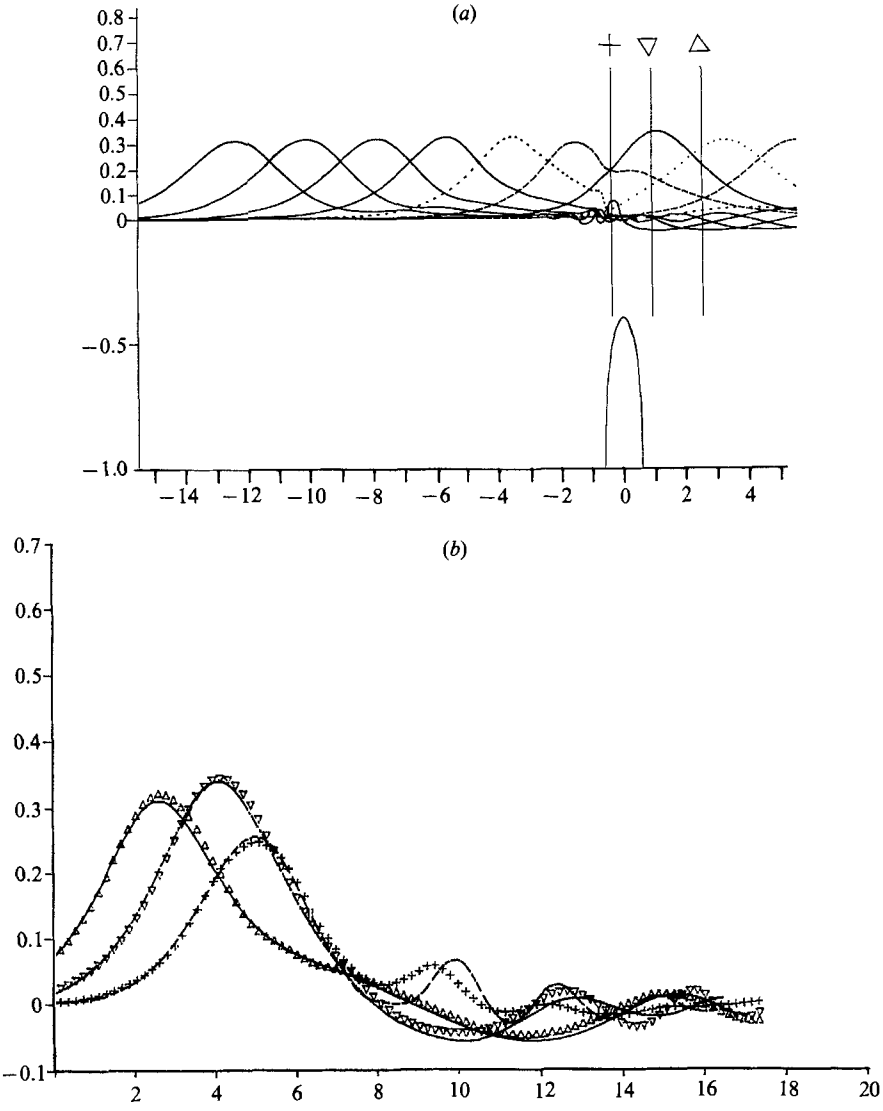

FIGURE 9. $a = 0.311$, $R = 0.6$. (a) Positions of experimental wave gauges and computed wave profiles. The symbol over each gauge corresponds to the symbol used in (b) to plot the gauge's record. Vertical exaggeration = 8. $t = 0, 2, 4, 6, \ldots, 16$. ($b$) Comparisons of experimental wave gauge records ($\nabla, \triangle, +$) with computations (——). Time increases along the x-axis in units of $(h/g)^{\frac{1}{2}}$.

The agreement is good between the predicted gauge responses and those measured in the experiments. The biggest discrepancy occurs at gauge position ∇ in figure 10(b) which is placed beyond the obstacle. The draw-down of the free surface near the obstacle has been over-predicted by 50% at gauge ∇ and this supports the inference that there was flow separation from the cylinder surface. We regret that no steps were taken to visualize this flow.

In this example the transmitted wave breaks (F-B in figure 2). The last profiles in figure 10(a) show strong surface steepening. This corresponds to the rapid rise in the water surface at time 6.5 in figure 10(b), at gauge positions ∇ and $+$.

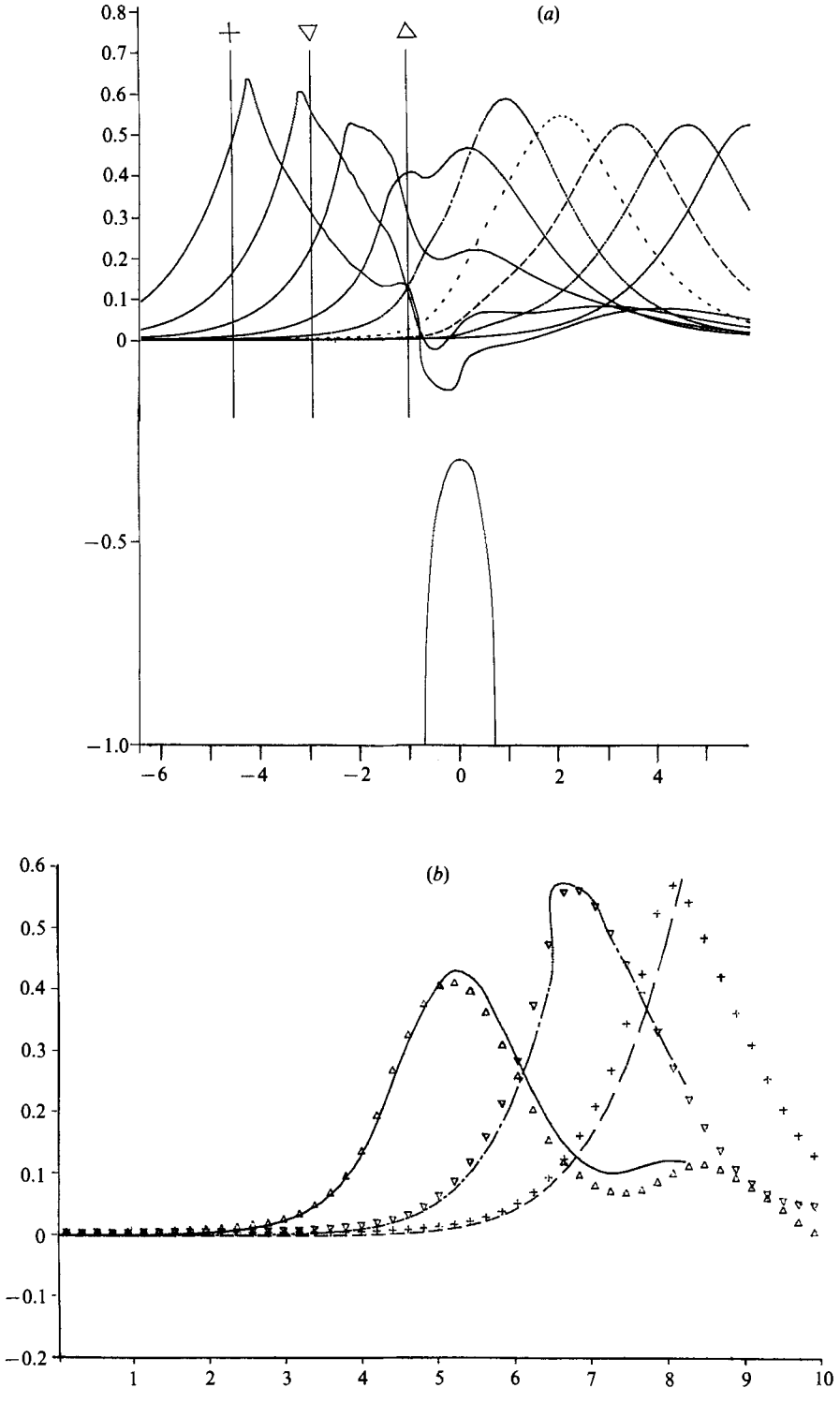

FIGURE 10. $a = 0.514$, $R = 0.7$. (*a*) Computed wave profiles and positions of wave gauges. Vertical exaggeration = 8. $t = 0, 1, 2, \ldots, 8$. (*b*) Comparison of experimental wave gauge records ($\triangle$, ∇, $+$) with computations (——).

The predictions stop at the moment the computations cannot resolve the surface motion. However, the video record allowed us to look at the waves beyond the last time of computation. Surprisingly, in this example the very steep surface of the backward breaker did not tip over, apart from slight spilling near the glass walls of the tank. Instead the wave (of approximate amplitude 0.08) passed back across the obstacle. This wave was followed by one further wave, which had an amplitude of approximately 0.04. So the waves behaved as though they were reflected from a point in the region of uniform topography, to the left of the obstacle. (This non-breaking motion is indicated more precisely by the smoothness of the wave record at $\triangle$ in figure 10(*b*), and by other gauges whose records are not presented here.)

These observations lend credence to the idea that the passage of a solitary wave over a cylinder induces a train of downstream stationary waves, which later become free to propagate and appear as reflected waves coming from beyond the cylinder. See the discussion of B-B in §3 above.

5.3. *Example* 3

The third example is for a cylinder of radius 0.8 and a wave height of 0.191. There is a backward breaker (corresponding to B-B in figure 2) and no forward breaking in the main crest.

Figure 11(*b*) shows the wave gauge responses. It is evident that the agreement between experiment and prediction is worst after time 7 at the gauge +, (which is in the trough of the backward breaker). The surface profiles in figure 11(*a*) show the exchange of crests across the obstacle, which corresponds, in figure 11(*b*) to the lower peak response of gauge + (at time 5) relative to the other gauges. There is also a deep draw-down of the free surface in front of the backward breaker, seen in gauge + near time 8. However, as in example 2, the video shows that the water surface steepened, but the wave did not break backwards. Again we suppose this lack of agreement may be due to separated flow behind the cylinder. In the computations the discretization points have been drawn apart by the flow near the backward breaker. There may be short stationary waves generated by the flow, not resolved by the computation-points, which may be why the numerical predictions are irregular.

6. Discussion

The (a, R) parameter space has been divided up into zones illustrated in figure 2, each of which has been separately discussed in §3. It is important to emphasize the fact that there are smooth transitions from one type of behaviour to another, in the (a, R) parameter space. Apart from W-T and C-C, all the regions are characterized by some breaking wave event, and as the parameters vary the breaking events smoothly change their position and timing.

In C-C the crest exchange is of principal importance, but the effect is seen over a much larger region of the parameter space. For example, the breaker F-B which occurs when R is 0.9 and a is 0.8 is an extreme form of crest exchange, in which the second crest breaks as it forms. If we reduce R from 0.9 then for wave amplitudes greater than 0.78 the second crest breaks further from the cylinder and we have Tanaka breaking T. For values of a between 0.6 and 0.78, as we reduce R from 0.9 to 0.8 the breaking in F-B changes from breaking near the obstacle to breaking far from the obstacle. If we reduce R still further, to around 0.7, the forward breaking occurs far beyond the obstacle, and is accompanied by backward breaking. If we also reduce a to around 0.6 then the backward breaking, B-B, occurs before the forward

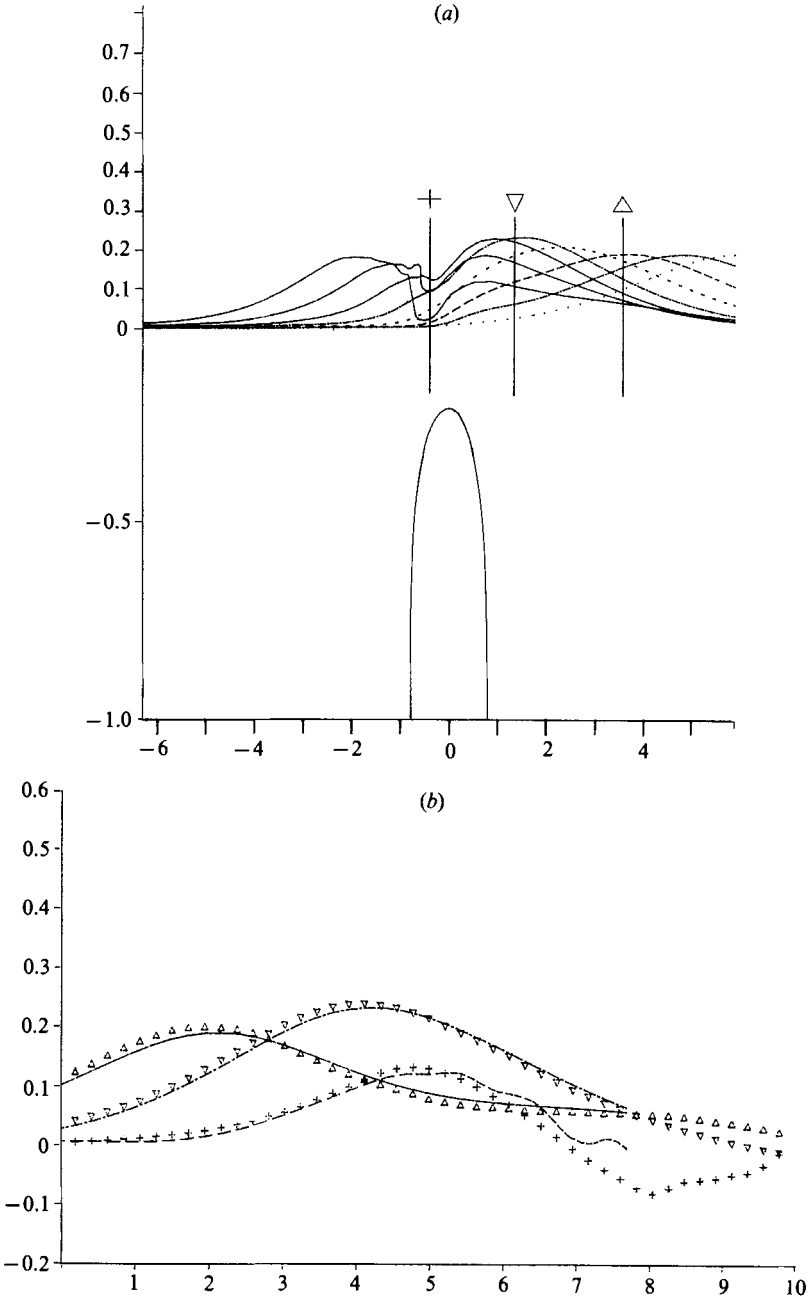

FIGURE 11. $a = 0.191$, $R = 0.8$. (*a*) Computed wave profiles and positions of wave gauges. Vertical exaggeration = 8. $t = 0, 1, 2, \ldots, 6$. (*b*) Comparison of experimental wave gauge records (∇, $\triangle$, +) with computations (——).

breaking. Further reductions in a or R correspond to wave motions without any breaking events, and the transmitted wave carries a wave train in its tail (W-T).

A solitary wave passes over a semicircle and induces a flow. If we allow a steady upstream current of speed c to flow over the same obstacle then for $R = 0.7$ and c less than approximately 0.2 a wave train occurs, and at certain higher flow rates a single

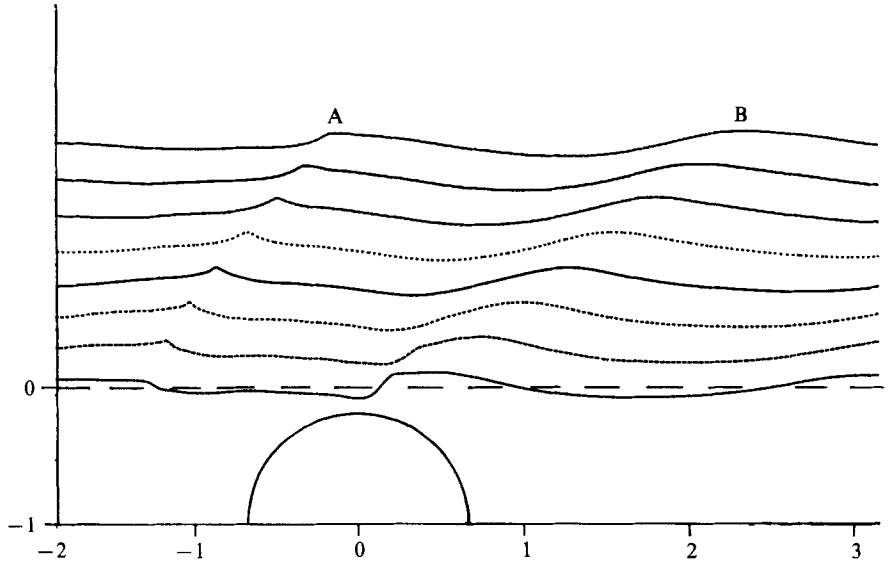

FIGURE 12. $R = 0.8$. Wave group passing over semicircle. Initial wave profile $y_0 = 0.1 \exp(-X^2/16) \sin(2X)$, and initial velocity potential $\phi_0 = 0.1 \exp(-X^2/16) \cos(2X)/c$, where $c^2 = \frac{1}{2}\tanh(2)$ and $X = x - 6.8$. $t = 10, 11, 12, \ldots, 17$.

backward breaking wave is seen downstream of the semicircle. Both types of disturbance are accompanied by a depression over the obstacle. The depression may correspond to the trough found between the two exchanged crests in C-C, and the downstream wave train may be related to the waves found in the wake of the transmitted wave in W-T. The higher flow rates give a backward breaking wave which appears to be similar to the B-B regime.

The experimental results are in good agreement with computation except behind the cylinder where flow separation may occur. This effect may be why observed surface disturbances in this region were smaller than expected, as occurred in example 2 of §5. However, the real fluid effects did not cause a different *type* of breaking from that computed. For times after those which we were able to compute, the video record shows many small-scale surface phenomena, probably influenced by the tank walls and by surface tension. Further experiments could look at other parts of the parameter space and investigate the importance of flow separation.

Since the above observations of solitary waves were not in accordance with our initial expectations, it is interesting to compare them with the motion of a group of periodic waves, travelling over the same semicircular obstacle. We consider an isolated group of waves which at time zero is symmetrically arranged about $x = 0$. The waves have sinusoidal profiles of wavelength π and the group is amplitude-modulated by $\exp(-x^2/16)$. The central, maximum crest height at $x = 0$ is 0.1, and there are five waves of significant amplitude in the group. Figure 12 shows the group propagating to the left towards a semicircle of radius 0.8, which is centred at $x = -6.8$. The waves preceding the largest pass over the obstacle without appreciable steepening. The central crest of the group, A, steepens over the front face of the semicircle and nearly breaks at time 12, but it recovers. The next wave in the group, B, which has amplitude less than the central maximum of 0.1, breaks shortly after the last profile of figure 12. The breaking of B occurs in a way that is reminiscent of

breaking on a beach or in shoaling water, and the motion is not at all like that of a solitary wave.

The wave group example shows that in a sequence of waves passing over an obstacle, each wave's interaction affects the next. The central wave A is able to surmount the obstacle, whereas its smaller successor B breaks. The breaking appears to be due to the backflow in the trough behind A. This sets up a counter-current over the semicircle against which B propagates and breaks. The presence of even small adverse currents at the obstacle may significantly affect whether or not breaking will occur.

In order to investigate the influence of currents on the solitary wave results reported above, we modified the program to model solitary wave motion over a semicircle, against a steady stream. The initial data consists of a solitary wave superposed on a flow over the semicircle, which has $y = 0$ and the bed contour as two of its streamlines. The initial position of the solitary wave was chosen close enough to the obstacle to avoid development of stationary waves downstream of the cylinder. The interaction between solitary and stationary waves has yet to be studied. For example a solitary wave, of height 0.5, propagates towards a semicircle of radius 0.5, and the steady stream flows from left to right, with speed c at infinity. When $c = 0$ the wave passes over the obstacle without breaking, but when $c = 0.2$ or 0.3 the current causes the wave to break. The wave still breaks beyond the cylinder.

These and a limited number of further computational examples suggest that (i) periodic waves differ from solitary waves, in that interactions in the obstacle neighbourhood cause breaking, and (ii) breaking of solitary waves is affected by an adverse current, but such breaking still occurs beyond the obstacle.

It is dangerous to draw any further conclusions from these examples since a number of new parameters are introduced. The amplitude and wavelength of the waves within the wave group can be varied, as can the initial position of the solitary wave, relative to the cylinder. Clearly, in order to come to definitive conclusions much more investigation of the multi-dimensional parameter spaces is needed.

7. Conclusions

In this paper we have described the extension of the Dold & Peregrine (1986) method from wave propagation in uniform depth to motion over a bump placed on a flat bed, whilst maintaining the efficiency of the program. Solitary waves are made to propagate over a semicircular obstacle, and the unusual surface motions were described in §3. The new phenomena we report for solitary waves are:

(*a*) a double crest when the wave is near the obstacle (C-C and in most of B-B and F-B in figure 2);

(*b*) a backwards breaker near the obstacle (B-B);

(*c*) waves appear to reflect from a region of uniform depth (B-B);

(*d*) when waves break they invariably break beyond the centreline of the semicircle (even when there is a small steady current flowing over the obstacle, against the oncoming wave);

(*e*) the incident crest breaks close to the obstacle only when the top of the semicircle is close to the surface.

The experiments described in §4 confirm crest–crest exchange and backward breaking. The comparisons in §5 show a reassuring quantitative agreement between our computations and the experimental results. The main discrepancies between

theory and experiment involve short-period oscillations near the back of the cylinder. It is suspected that the flow separated from the cylinder surface.

Some of the features described in this paper, especially those concerning reflected waves, may be related to the waves generated by steady flow over a semicircular cylinder. The principal waves generated by the steady flow, in its initial evolution, discussed under C-C, are about the same size as the disturbances induced by the solitary waves. Large solitary waves ($a > 0.6$) are well-described by our numerical method, but they are difficult to make in the laboratory. Consequently both Tanaka's (1986) instability, and its presence in the region T, await experimental confirmation. The phenomenon (*e*) could be checked by making the water over the obstacle very shallow. Even a moderate wave should be able to induce a breaker. We find that periodic waves in the presence of an obstacle exhibit a response that differs from that of solitary waves. An adverse current affects whether or not a solitary wave will break, but any breaking still occurs beyond the obstacle.

Many thanks to Professor M. Losada for permission to use the wave tank at Santander University, Spain. Thanks also to M. Lewy for his help with the computer programming, and A. F. Teles da Silva for program testing. Financial support for M. J. Cooker from the UK Science and Engineering Research Council, is acknowledged.

REFERENCES

Dold, J. W. 1990 An efficient surface-integral algorithm for unsteady water waves. In preparation.

Dold, J. W. & Peregrine, D. H. 1986 An efficient boundary-integral method for steep unsteady water waves. In *Methods for Fluid Dynamics II* (ed. K. W. Morton & M. J. Baines), pp. 671–679. Oxford University Press.

Evans, D. V. & Linton, C. M. 1989 Active devices for the reduction of wave intensity. *Appl. Ocean Res.* **11**, 29–32.

Forbes, L. K. & Schwartz, L. W. 1982 Free-surface flow over a semi-circular obstruction. *J. Fluid Mech.* **114**, 299–314.

New, A. L. 1983 On the breaking of water waves. Ph.D. thesis, University of Bristol, UK.

New, A. L. & Dyer, K. R. 1988 Internal waves and mixing in stratified estuarine flows. In *Physical Processes in Estuaries* (ed. J. Dronkers & W. van Leussen), pp. 239–254. Springer.

New, A. L., Dyer, K. R. & Lewis, R. E. 1986 Predictions of the generation and propagation of internal waves and mixing in a partially stratified estuary. *Estuar. Coast. Shelf Sci.* **22**, 199–214.

New, A. L., Dyer, K. R. & Lewis, R. E. 1987 Internal waves and intense mixing periods in a partially stratified estuary. *Estuarine Coastal Shelf Sci.* **24**, 15–33.

Peregrine, D. H. 1990 The surface of steep unsteady water waves. In *Mathematics and Computation of Deforming Surfaces* (ed. J. C. R. Hunt). Oxford University Press (to appear).

Seabra-Santos, F. J., Renouard, D. P. & Temperville, A. M. 1987 Numerical and experimental study of the transformation of a solitary wave over a shelf or isolated obstacle. *J. Fluid Mech.* **176**, 117–134.

Tanaka, M. 1986 The stability of solitary waves. *Phys. Fluids* **29**, 650–655.

Tanaka, M., Dold, J. W., Lewy, M. & Peregrine, D. H. 1987 Instability and breaking of a solitary wave. *J. Fluid Mech.* **185**, 235–248.

Teles da Silva, A. F. 1989 Applications of boundary-integral methods to the study of steep free-surface waves, Ph.D. thesis, University of Bristol, UK.

Vinje, T. & Brevig, P. 1981 Nonlinear ship motions. *3rd Intl Conf. on Numerical Ship Hydrodynamics, Paris, France.*

Yasuda, T., Hara, M. & Tanaka, M. 1990 A computational model of the deformation including overturning of a solitary wave over a submerged obstacle. *Wave Motion* (submitted).